Comparison of regional carbon flux estimates from CO_2 concentration measurements and remote sensing based footprint integration

Baozhang Chen,[1] Jing M. Chen,[1] Gang Mo,[1] and T. Andrew Black[2]

Received 1 June 2007; revised 7 September 2007; accepted 7 December 2007; published XX Month 2008.

[1] Quantification of terrestrial CO_2 sources and sinks at regional scales ($\sim 10^2 - 10^6$ km^2) is fundamental to improving our understanding of the terrestrial carbon cycle. Two independent methods to extract the gross primary productivity (GPP) from atmospheric CO_2 concentration measurements were explored and compared in this study. The methods were (1) planetary boundary layer (PBL) carbon budget analysis that allows the estimation of regional GPP at daily time steps from hourly CO_2 concentration measurements and (2) spatially explicit hourly carbon cycle modeling based on remote sensing and then integrating the daily flux field with a concentration footprint function depending on wind and stability. These methods have been applied to a 28-m tower at an old black spruce site near White Swan Lake (~100 km NE of Prince Albert: 53.98717°N, 105.11779°W). The estimates of daily GPP by these two approaches agreed well for 2003 (slope = 0.99; r^2 = 0.89). In order to test these methods of inferring the regional GPP from mixing ratio measurements, we also compared the estimates of regional GPP with estimates made using eddy covariance (EC) flux measurements, although their respective source areas are different. They had similar seasonal patterns, but the regional estimates were consistently smaller than the local EC flux derived GPP throughout the growing season in 2003. These estimates of annual regional GPP were 649–664 g C m^{-2} for 2003 while the EC-derived annual GPP was 819–847 g C m^{-2}. The annual difference was about 20–25%. The EC flux footprint of the tower was relatively homogeneous old black spruce while the concentration footprint, which was a few orders of magnitude larger than the flux footprint, covered boreal evergreen and deciduous broadleaf forests, grassland, cropland, and lakes. Nonforested land occupied about 10–50% of the concentration footprint depending on wind direction and speed and was less productive than the black spruce forest. The discrepancies between regional and local GPP estimates reflected the differences in underlying land surfaces represented by the different footprint areas.

Citation: Chen, B., J. M. Chen, G. Mo, and T. A. Black (2008), Comparison of regional carbon flux estimates from CO_2 concentration measurements and remote sensing based footprint integration, *Global Biogeochem. Cycles*, *22*, XXXXXX, doi:10.1029/2007GB003024.

1. Introduction

[2] Ecosystem functioning and its role in the carbon balance are much better understood than before as a result of measuring and analyzing energy and CO_2 fluxes made at sites using the eddy covariance (EC) technique [*Baldocchi et al.*, 2001]. Direct measurements of the terrestrial carbon flux using these techniques have nearly continuous temporal coverage at an increasing number of sites across continents [*Black et al.*, 1996; *Baldocchi et al.*, 2001]. EC measurements are a rich source of information on temporal variability and environmental controls of CO_2 exchange between the atmosphere and terrestrial ecosystems [*Law et al.*, 2002]. However, EC measurements under Fluxnet programs represent only a very small fraction of the land area, typically less than 1–3 km^2 for each site.

[3] The atmosphere integrates surface fluxes over many temporal and spatial scales and links scalar sources and sinks with concentrations and fluxes. This principle has been successfully used to develop inverse models to estimate annual carbon budgets [*Tans et al.*, 1990; *Enting et al.*, 1995; *Fan et al.*, 1998; *Bousquet et al.*, 1999; *Gurney et al.*, 2002]. However, because of model limitations and paucity of continental CO_2 observations these studies have yielded carbon fluxes only at coarse resolution, over large spatial regions (i.e., at continental scale [*Rodenbeck et al.*, 2003]).

[4] Progress in carbon balance studies has been achieved at the extreme ends of the spatial-scale spectrum, either

[1]Department of Geography and Program in Planning, University of Toronto, Ontario, Canada.

[2]Biometeorology and Soil Physics Group, Faculty of Land and Food Systems, University of British Columbia, Vancouver, British Columbia, Canada.

0886-6236/08/2007GB003024$12.00

large continents (larger than 10^6 km^2, e.g., global inverse modeling) or small vegetation stands (less than 1–3 km^2, e.g., EC measurements). Methods to estimate CO_2 sources and sinks at the intermediate scale between continental and local scales are notably lacking. Moreover, the carbon cycle in different regions can vary markedly in response to changing climate [*Friedlingstein et al.*, 2003; *Fung et al.*, 2005]. Reliable estimates of terrestrial CO_2 sources and sinks at intermediate spatial scales (finer than those used in global inversions and larger than local EC flux measurements and roughly defined as the range between 10^2 and 10^6 km^2) are required to quantitatively account for the large spatial variability in sources and sinks in the near-field of a measurement location [*Gerbig et al.*, 2003], as well as fundamental to improving our understanding of the carbon cycle [*Crevoisier et al.*, 2006].

[5] It is extremely unreliable to upscale stand-level fluxes (i.e., EC measurements) to a region by simple spatial extrapolation and interpolation because of the heterogeneity of the land surface and the nonlinearity inherent in ecophysiological processes [*Levy et al.*, 1999]. It is also challenging to apply atmospheric inversion technique to regional scales for quantifying annual carbon budgets because at such intermediate scales the atmosphere is often poorly constrained [*Gloor et al.*, 1999; *Matross et al.*, 2006]. Moreover, aggregation errors and errors in atmospheric transport, both within the boundary layer and between the boundary layer and free troposphere, can also be formidable obstacles to using these approaches to obtain quantitative estimates of regional carbon fluxes [*Lin et al.*, 2006]. Hence, there is a strong motivation to develop methods to use atmospheric observations to quantify and validate estimates of the carbon balance at these intermediate scales [*Lin et al.*, 2006; *Bakwin et al.*, 2004; *Matross et al.*, 2006; *J. M. Chen et al.*, 2007]. Observations of CO_2 over the continent within the atmospheric boundary layer reflect exchange processes occurring at the surface at a regional scale (10^2–10^5 km^2). The flux information contained in CO_2 concentration data represents footprints of up to 10^5 km^2 [*Gloor et al.*, 2001; *Lin et al.*, 2004], which are several orders of magnitude larger than the direct EC flux footprint. This information is therefore much needed in our effort to upscale from site to region. Moreover, the number of CO_2 mixing ratio measurements above the land surface, made by either tower or aircraft, is steadily increasing. Previous efforts to interpret the signal of regional CO_2 exchange making use of tower concentration data have focused on simple one-dimensional planetary boundary layer (PBL) budgets that rely on gradients in CO_2 concentrations between the boundary layer and the free troposphere [*Bakwin et al.*, 2004; *Helliker et al.*, 2004]. These methods are limited to monthly resolution because of the need to smooth and average over several synoptic events [*Matross et al.*, 2006].

[6] The objective of this study is to explore pragmatic and reliable methods to extract the gross primary productivity (GPP) from atmospheric CO_2 concentration measurements on the basis of PBL analysis. Making use of an integrated ecosystem-boundary layer model for simulating ecosystem fluxes and atmospheric diffusion [*Chen et al.*, 2004], we have previously developed a PBL carbon budget methodology that allows the estimation of regional GPP on a daily basis from hourly concentration measurements [*B. Chen et al.*, 2006a, 2006b; *J. M. Chen et al.*, 2007]. As part of this study, we develop another novel methodology to retrieve regional GPP by superimposing the daily concentration footprint on the underlying daily GPP field simulated using a spatially explicit ecosystem model driven by remote sensing inputs. The comparisons of these two independent regional GPP estimates, i.e., one is concentration derived and the other is concentration footprint integrated, have been made for a 28-m tower at an old black spruce site near White Swan Lake, Saskatchewan Canada. From this study, we seek to address the following questions. (1) How well do the estimates of regional GPP from these two independent methods match each other? (2) How well do both methods of deriving regional GPP compare with EC-derived local GPP and what are the reasons? (3) Are these methodologies applicable to retrieving other components of the terrestrial carbon cycle (i.e., net ecosystem productivity F_{NEP} and ecosystem respiration R)?

2. Materials

2.1. Study Site Descriptions

[7] The research site (53.98717°N, 105.11779°W, and 629 m above the sea level) is located approximately 100 km NE of Prince Albert, Saskatchewan, Canada. It is referred to as Southern Old Black Spruce (SOBS) and was established in 1994 as past of the Boreal Ecosystems Atmosphere Study [*Sellers et al.*, 1997]. The EC flux footprint area is dominated by black spruce (*Picea mallana Mill.*) but approximately 15% of the forest consists of deciduous tamarack (*Larix laricina* (DuRoi) K. Koch). The height of the dominant trees is 11 m. The stand density is ~6350 stems per hectare. Its leaf area index (LAI) is about 3.5–3.8 m^2 m^{-2}. The last disturbance occurred in 1879. Some Labrador tea (*Ledum groenlandicum* Oeder) is in the understory with a ground cover of mostly feathermoss (*Pleurozium spp.).* This forest is located in a boggy area with many small pockets of standing water. The landscape in the region is predominantly flat, with slight topographical undulations. On the basis of a 40-year climate record made at Waskosia Lake station, the mean annual and growing season (May to September) air temperatures in the region are 1.0°C and 13.4°C, respectively, and the mean annual precipitation is approximately 440 mm, of which 40% falls as snow. This site has an elevated water table and is generally wet. The texture of the mineral soil is sandy clay. The surface organic layer is 20–30-cm thick and carbon storage in this layer is 39.2 kg C m^{-2}. Further site details are given by *Jarvis et al.* [1997], *Griffis et al.* [2003], and *Kljun et al.* [2006].

2.2. Land Surface Characteristics of the Concentration Footprint

[8] The daily concentration footprint areas of the 28-m tower accumulated for a year could be as large as a circle around the tower up to a 350-km radius (see section 4.2). As shown in Figures 1 and 2, the areas within the footprint are

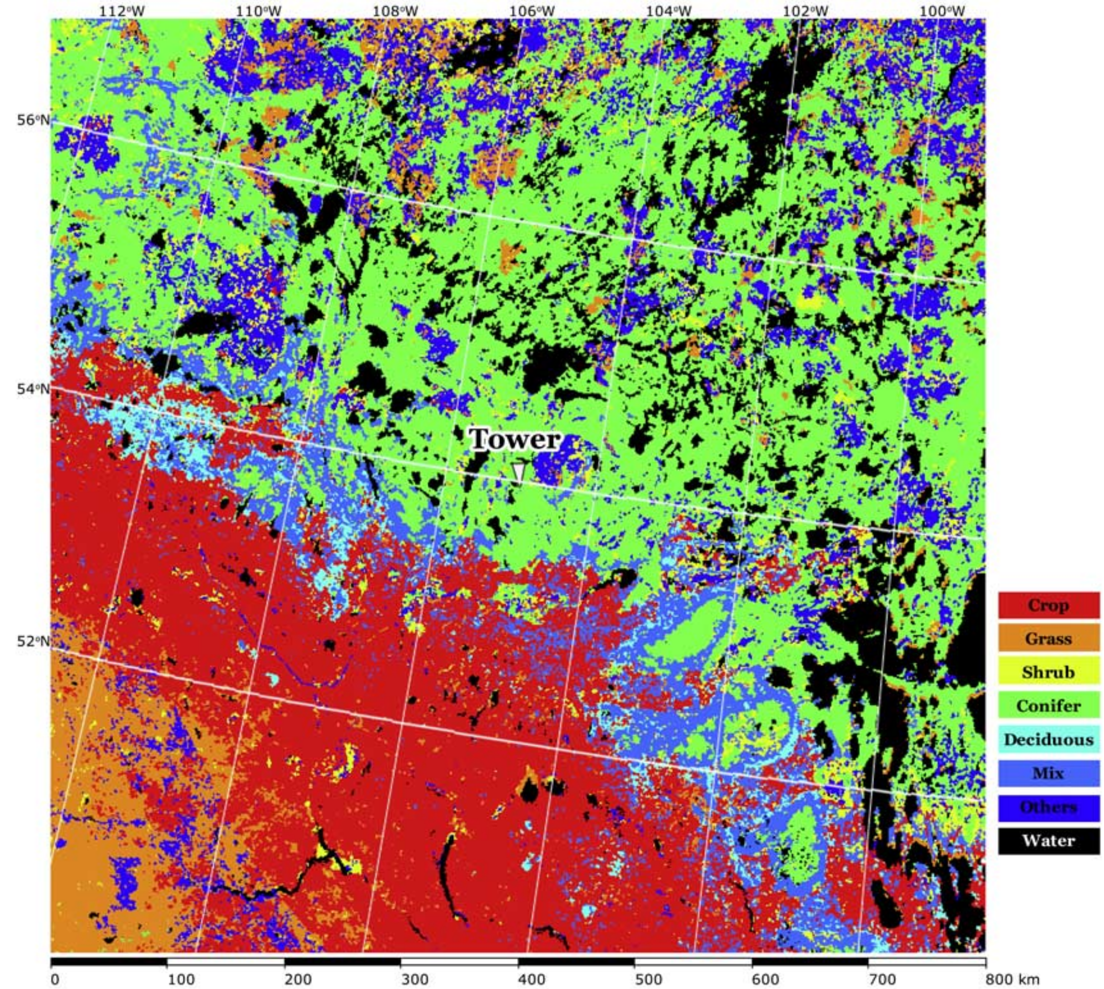

Figure 1. Land cover types around the SOBS tower for 2003.

quite heterogeneous. Land cover types (LC) in these areas include conifer forest, deciduous forest, mixed forest, shrub, grass, crop, and nonvegetation type (Figure 1). The dominant LC is conifer forest around the tower within a 100-km radius; while the area to the southeast (>180 km from the tower) is dominated by grass or crop types. The dominant LC types of deciduous and mixed forests are located in the areas to the southeast and southwest from the tower between ∼100 and ∼180 km. Figure 2 shows a LAI map for August 2003, as an example. LAI varied from 0.5 to 8 m^2 m^{-2} in the footprint. The LAI for the area surrounding the tower within a 100-km of radius was ∼3.5–4.5 m^2 m^{-2}.

2.3. EC and CO_2 Concentration Measurements

[9] Half-hourly CO_2 and water fluxes and other meteorological variables at this site were measured on a 28-m walk-up scaffold tower using the EC technique. The EC instruments were mounted at the 25-m height. They included a three-dimensional sonic anemometer-thermometer (model R3; Gill Instruments Limited, United States; Lymington, UK) and a closed-path infrared gas analyzer (model 6262; LI-COR Incorporated, Lincoln, Nebraska, United States) operating in absolute mode for measuring fluctuations in CO_2 and water vapor density. Details about the EC system are given by *Black et al.* [1996], *Arain et al.* [2002], and *Griffis et al.* [2003].

[10] CO_2 concentration was measured at both the 20-m and 28-m heights according to World Meteorological Observation (WMO) Global Atmospheric Watch standards with an accuracy of 0.1 ppm at 15 min intervals. Calibrations using a WMO standard were made at approximately 1-week intervals. Gaps with no valid data at any level were less than 10% year round. Small data gaps of 1 to 2 h were filled by linear interpolation.

3. Methods

3.1. Model Framework and Assumptions

[11] Meteorological processes such as the entrainment of tropospheric air during boundary layer growth, synoptic-scale subsidence of the troposphere, radiative processes, mesoscale circulations (e.g., sea/lake breezes) and boundary layer cloud formulation tend to counter the influence of the land surface by facilitating mixing between the PBL and the typically drier and warmer overlying troposphere [*Helliker et al.*, 2004]. The PBL air mass moves over the terrestrial

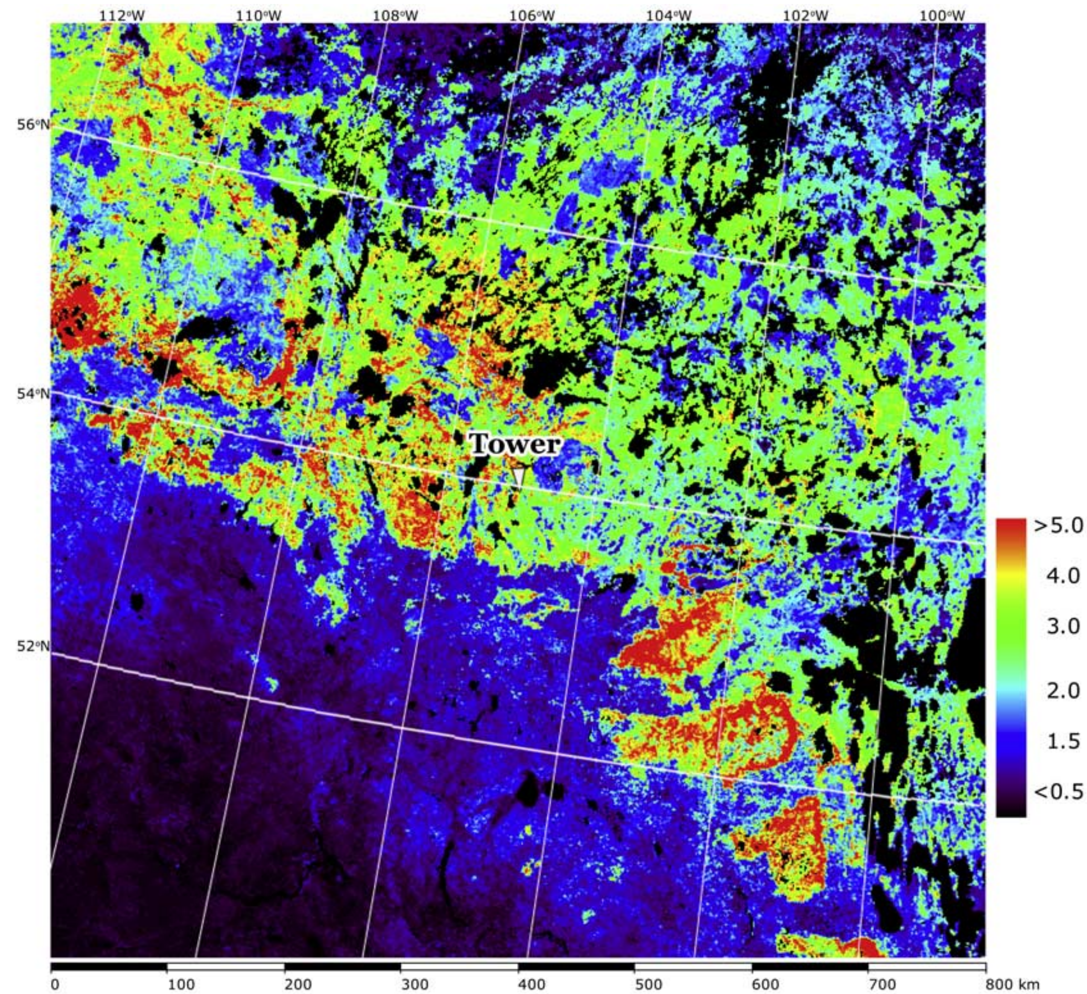

Figure 2. Leaf area index (LAI) map for the region surrounding the SOBS tower for the first 10 d of August 2003.

surface (~500 km d^{-1} under typical fair weather conditions), dispersing trace gases horizontally and vertically due to divergence and wind shear [*Raupach et al.*, 1992]. Hence, the air composition in the surface layer is determined by the initial composition of the air mass and the exchanges with the underlying surface and the overlying free troposphere [*Helliker et al.*, 2004]. It has been noted from three-dimensional atmospheric transport model simulations [e.g., *Fung et al.*, 1983] that meridional transport can result in substantial displacement of the actual change in the atmospheric burden of CO_2 in latitudinal zones from the corresponding surface fluxes that drove them. The influence of large-scale atmospheric transport on CO_2 concentration in the atmospheric boundary layer is hence expected, and this should interact with concentration gradients generated by regional exchange with the surface. Suppose we want to estimate surface fluxes in a given region (e.g., the daily concentration footprint area), on the basis of mass conservation, the atmospheric concentration of a gas (e.g., CO_2, expressed as C) measured in a terrestrial tower at a reference height (observed values, i.e., in the land surface layer) reflects the combination of some background atmospheric concentration and variable amounts of that gas added from sources in both the vertical and horizontal directions:

$$C_{\text{obs}} = C_{\text{bg}} + \Delta C_{\text{surf}} + \Delta C_{\text{adv}}, \qquad (1)$$

where C_{obs} and C_{bg} are, respectively, the observed atmospheric CO_2 concentration at a reference site and the background value; ΔC_{surf} is the change in the CO_2 mixing ratio caused by local surface fluxes of carbon, which might result mostly from local biological activities, biomass burning and the fossil fuel combustion; ΔC_{adv} is the change in the CO_2 mixing ratio due to advection resulting from a horizontal CO_2 gradient. Equation (1) works in many time frames, e.g., hourly, daily, and monthly. The CO_2 mixing ratios in terrestrial ecosystems are also found to be dominated by biological activities during the growing season under the condition that the upwind ecosystems behave in a very uniform way [*Bakwin et al.*, 1998; *Potosnak et al.*, 1999]. In this study, we tried to explore a simple method to infer regional GPP in daily time steps from continuous CO_2 mixing ratio measurements in the surface layer using a 1-D model. We therefore assume that ΔC_{adv} can be ignored since $\Delta C_{surf} \gg \Delta C_{adv}$ in the daily short time frame.

[12] The boundary layer interacts with the surface (including horizontal advection) and the background atmosphere on similar time frames. While changes in the atmospheric background CO_2 by many factors, such as advection, deep convection, subsidence, etc., are normally much slower than that in measured surface CO_2. The relaxation time of changes in the background atmospheric CO_2 (i.e., the CO_2 concentration in free troposphere in this study) is much longer than that in the PBL driven by the exchange of CO_2 with the surface in the daily concentration footprint area (about 1 order longer, e.g., 10 d versus 1 d). Hence, the background CO_2 changes could be ignored.

[13] We also neglected the difference between the free tropospheric CO_2 value and value observed within the marine boundary layer ("MBL reference"). The MBL reference CO_2 [*Masarie and Tans*, 1995] is a weekly varying concentration field with spatial increment of 0.05 sine of latitude constructed from observations within the MBL [*Globalview-CO*$_2$, 2005]. We used the MBL reference for free troposphere because of the absence of direct observations, though observations from the high observational density from intensive field sampling programs showed significant deviations of free tropospheric concentrations from the MBL references in some regions over the continent. However, during the daytime, the change in free tropospheric CO_2 is expected to be small. It is the daytime change that affects the deviation of daily GPP.

3.2. Method 1: PBL Carbon Budget Analysis

3.2.1. An Integrated Ecosystem-Boundary Layer Model for Estimating Ecosystem Fluxes and Atmospheric Diffusion

[14] In order to isolate photosynthesis signals from atmospheric CO_2 data, we employed an integrated ecosystem-boundary layer model to simulate dynamics of CO_2 in the PBL. This model consists of two components: (1) an ecosystem model (BEPS: the Boreal Ecosystem Productivity Simulator) [*Chen et al.*, 1999; *Liu et al.*, 1999, 2002]; and (2) a one-dimensional atmospheric model (VDS: Vertical Diffusion Scheme) [*Chen et al.*, 2004; *B. Chen et al.*, 2005].

[15] The version of BEPS used in this study is a new version that includes a land surface scheme: Ecosystem-Atmosphere Simulation Scheme (EASS) [*B. Chen et al.*, 2007]. It has the following characteristics: (1) satellite data are used to describe the spatial and temporal information on vegetation, and in particular, we use a foliage clumping index (Ω) in addition to LAI to characterize the effects of three-dimensional canopy structure on radiation, heat and carbon fluxes; (2) energy and water exchange and carbon assimilation in soil-vegetation-atmosphere systems are fully coupled and are simulated simultaneously; and (3) the energy and carbon assimilation fluxes were calculated with stratification of sunlit and shaded leaves to avoid shortcomings of the "big-leaf" assumption. This updated version has been systematically validated using eddy covariance flux data [*Ju et al.*, 2006; *B. Chen et al.*, 2007] at Canadian forest sites and used for upscaling land surface fluxes [*J. M. Chen et al.*, 2007] and isotope studies [*B. Chen et al.*, 2006a, 2006b; *Chen and Chen*, 2007].

[16] VDS is a one-dimensional bottom-up and top-down vertical mixing model [*Chen et al.*, 2004; *B. Chen et al.*, 2005] similar to those of *Wyngaard and Brost* [1984] and *Moeng and Wyngaard* [1989] simulating the transport processes of scalar entities (e.g., CO_2, temperature) from the surface layer up to the top of PBL. VDS has two different schemes (modules) to treat different situations of the PBL structures (stable boundary layer: SBL or convective boundary layer: CBL) [*Chen et al.*, 2004; *B. Chen et al.*, 2005]. The selection of a stable or free convection scheme is determined by atmospheric stability. In VDS, the mixed layer is stratified into 50-m thick layers and constant bottom-up and top-down mixing coefficients are used throughout the PBL at a given time [*Zhang and Anthes*, 1982]. This model configuration allows CO_2 concentration in each layer to vary with time according to the vertical concentration gradient and the mixing coefficients at each time step (30 s) in stead of using the quasi-steady state assumption for the vertical gradient [*Moeng and Wyngaard*, 1989]. The integrated ecosystem-boundary layer model is forced by the near-surface meteorological variables, including air temperature, air relative humidity, incoming shortwave radiation, wind speed, and precipitation. The land surface data, including vegetation (i.e., LC, LAI) and soil data are also needed as model inputs. Most vegetation parameters were derived from satellite images. As shown in Figures 1 and 2, LC and LAI were derived from satellite images at a 1-km resolution (directly from VEGETATION images, or up-scaling from Landsat TM) [*Chen et al.*, 2002]. The LAI map is generated with 10-d intervals with annual total of 36 maps. Ω was derived from multiangular POLDER 1 data [*J. M. Chen et al.*, 2005]. Data on soil texture (sand, silt and clay fractions) and carbon pools are obtained from the Soil Landscapes of Canada (SLC) database, version 1.0 and 2.0 [*Shields et al.*, 1991; *Schut et al.*, 1994; *Lacelle*, 1997]. For the one-dimensional BEPS-VDS simulations, the average values of LAI and Ω near the OBS (a radius of 1 km) are obtained from these maps, and the LC type is taken as the dominant type of conifer. For estimating the entrainment of CO_2 at the top of the mixed layer, the background atmospheric value (i.e., the free tropospheric CO_2) is needed for the top condition of our one-dimensional model. As mentioned above, we use the latitudinally interpolated MBL CO_2 as a substitute for the free troposphere.

3.2.2. Method for Deriving Daily GPP From CO_2 Concentration Measurements

[17] As the air CO_2 mixing ratio at a given height is determined by both the surface metabolism and atmospheric mixing processes. It would be possible to isolate the signals for the metabolism if atmospheric diffusion is accurately modeled. This requires that both the exchange of CO_2 between the ecosystem and the atmosphere and the atmospheric transport within the PBL are accurately simulated. This integrated ecosystem-boundary layer model (BEPS-VDS) simulated well the surface fluxes (both photosynthesis and respiration) and the concentration of CO_2 in the surface layer (see section 4). After the first "normal" model run, we implement a hypothetical model run by switching

off GPP in the model, i.e., setting GPP = 0. In the this run, only the GPP produced by BEPS is set to zero while keeping all other hourly fluxes unchanged from the previous run, including respiration and entrainment. A new CO_2 profile produced in the second model run is purely driven by R, which is simulated by BEPS for the grid cell around the tower. The reduction of observed CO_2 from the simulated values at the measurement height is entirely due to GPP, that is, the amount of the reduction is the part of CO_2 removed by GPP. The signals of GPP are hence isolated by "turning off" the GPP in BEPS and quantifying the accumulated air CO_2 decrease (the difference between the observed and simulated values with GPP = 0) from dawn to dusk. Near dusk, the planetary boundary layer is still well mixed, so this increase in CO_2 can be converted into GPP using boundary layer CO_2 mass budgeting. This methodology has been applied to a 13-year CO_2 record observed on the Fraserdale tower, Ontario, Canada, to study the temperature effect on the boreal carbon cycle [*B. Chen et al.*, 2006a, 2006b] and validated using simultaneous CO_2 flux and concentration data at the WLEF tall tower (Wisconsin, United States [*J. M. Chen et al.*, 2007]).

3.3. Method 2: Remote Sensing Based Footprint Integration

3.3.1. An Analytical Scalar Concentration Footprint Model

[18] The scalar concentration footprint "source" area is the "view of the concentration sensor" on a tower. The scalar concentration footprint function (f) describes the flux portion "seen" by the scalar concentration sensor. Our concentration footprint model is a modified version of that of *Schmid* [1994]. All upwind sources encompassed by the measurement point at a height (z_m) above the ground potentially contribute to the measured scalar concentration (C). The measured departures of CO_2 concentration from the background values C_{bk}, therefore, is the result of an integration of the product of the surface flux (F, in μmol m^{-2} s^{-1}) and footprint function (f) over the entire upwind source area:

$$C(0,0,z_m) = C_{bk} + \int_{-\infty}^{\infty}\int_{-\infty}^{\infty} F(x,y,0) f(x,y,z_m) dxdy, \quad (2)$$

where C is in μmol m^{-3}; f is in s m^{-3}; x is the stream-wise distance in meters; and y is the crosswind distance from the center line in meters.

[19] The scalar concentration footprint function (i.e., the downwind concentration distribution of a unit point source (plume) occurring at the origin ($x = y = 0$, $z \geq 0$)) is the product of the crosswind-integrated concentration footprint, f^y in s m^{-2}, and the crosswind distribution function D_y in m^{-1} [*Pasquill*, 1974; *van Ulden*, 1978; *Horst and Weil*, 1992],

$$f(x,y,z_m) = D_y(x,y) f^y(x,z_m). \quad (3)$$

Dispersion in the lateral (y) direction is calculated as a Gaussian function [*Pasquill*, 1974],

$$D_y(x,y) = \frac{1}{\sqrt{2\pi}\sigma_y} \exp\left(-\frac{y^2}{2\sigma_y^2}\right), \quad (4)$$

where σ_y is the standard deviation of the plume in the y dimension, depending on atmospheric stability and upwind distance (x). In accordance with the short-range limit of statistical turbulence theory [*Pasquill*, 1974; *Schmid*, 1994], σ_y is approximated as $\sigma_v x/\bar{u}$, where σ_v is the standard deviation of lateral wind fluctuations.

[20] The crosswind-integrated concentration footprint, f^y at the upwind distance x is described as

$$f^y(x,z_m) = \frac{D_z(x,z_m)}{\bar{u}(x)}, \quad (5)$$

where D_z is the vertical concentration distribution function in m^{-1} and $\bar{u}$ is the effective velocity of the plume in m s^{-1}; $\bar{u}$ is forced by mass conservation to be

$$\bar{u}(x) = \int_0^{\infty} u(z) D_z(x,z) dz, \quad (6)$$

where u(z) is the horizontal wind velocity in m s^{-1}. Following an analytical solution of Eulerian advection-diffusion equation by *van Ulden* [1978], D_z is expressed as

$$D_z(x,z_m) = \frac{A}{\bar{z}(x)} \exp\left[-\left(\frac{Bz}{\bar{z}(x)}\right)^r\right], \quad (7)$$

where $\bar{z}$ is the mean plume height; the coefficients A and B equal $r\Gamma(2/r)/\Gamma(1/r)^2$ and $\Gamma(2/r)/\Gamma(1/r)$, respectively; Γ is the Gamma function and r is a shape parameter and $r = 2 + m - n$, where m and n are the exponent of the wind velocity power law and the exponent of the eddy diffusivity power law, respectively; $u(z) = Uz^m$ and $K(x) = kz^n$, where U and k are the effective speed of plume advection and an effective eddy diffusivity coefficient, respectively. For mathematical simplicity, we need to explicitly express $\bar{z}(x)$ and $\bar{u}(x)$ to solve equations (5) and (7) by integration of equation (13) of *van Ulden* [1978] as

$$\bar{z}(x) = B\left(\frac{r^2 k}{U}\right)^{1/r} x^{1/r}, \quad (8a)$$

$$\bar{u}(x) = \frac{\Gamma((1+m)/r)}{\Gamma(1/r)} \left(\frac{r^2 k}{U}\right)^{m/r} U x^{m/r}. \quad (8b)$$

[21] This is a very Simple Analytical Footprint model on Eulerian coordinates (SAFE). On the basis of the K-theory and assuming horizontally homogeneous turbulence, an analytical solution of $f(x, y, z_m)$ is obtained from the functional form of the concentration distribution and the shape of the wind profile (equation (3)). The dimensions and orientation of $f(x, y, z_m)$ depend on the location and

height of the sensor, wind direction, wind velocity, surface roughness, and atmospheric stability.

[22] Footprint estimates can be classified as stochastic Lagrangian, analytical approaches, or large-eddy simulations. Lagrangian models can be applied in any turbulence regime (even in inhomogeneous or nonstationary conditions), while most analytical models are constrained to homogeneous turbulence. The values of the upwind tail of concentration footprint estimated by a three-dimensional Lagrangian stochastic dispersion model are generally higher than those by an analytical footprint model [*Kljun et al.*, 2003]. At these large separation distances between the source and the receptor, the mean plume height could be well above the surface layer, and thus beyond the validity range of the K-theory-based analytical model. To avoid the model biases resulting from the limitation of our analytical model, we neglected the very small contribution from the long upwind tail. In the model implementation, we simply sort $f(x, y, z_m)$ values in a descending order and then accumulate the values from the largest to the smallest until a given fraction Π is achieved. The source area Ω_Π includes all grids (pixels) that have $f(x, y, z_m)$ larger than the cutoff point, and the fraction Π is the ratio of the cumulative footprint function within Ω_Π to the whole integrated source function,

$$\Pi = \frac{\varphi_P}{\varphi_{\mathrm{tot}}} = \frac{\iint_{\Omega_P} f(x,y,z)dxdy}{\int_{-\infty}^{\infty}\int_{-\infty}^{\infty} f(x,y,z)dxdy}, \qquad (9)$$

where φ_P and φ_{tot} are the integrals of the footprint function over Ω_Π and the total area, respectively. In this study, we set Π to 0.90. The footprint function $f(x, y, z_m)$ at every grid point within Ω_Π is then normalized by the integral of the footprint function over Ω_Π for each day to yield the daily weighted footprint function (ϕ),

$$\phi(x,y) = f(x,y,z_m)dxdy \Big/ \iint_{\Omega_P} f(x,y,z_m)dxdy. \qquad (10)$$

The integral of daily weighted footprint function (ϕ) equals 1.

[23] The SAFE model was coupled with EASS. The sensible heat flux simulated by EASS is needed for calculating the atmospheric stability in SAFE. SAFE needs the same model inputs as BEPS (see section 3.2.1) with the additional input of hourly wind direction and its deviation.

3.3.2. Method of Calculating Regional Carbon Fluxes on the Basis of Footprint Estimation and Ecosystem Modeling

[24] The surface flux information contained in CO_2 concentration measured at the tower (F_{region}) is the integration of surface CO_2 flux (F) weighted with concentration footprint function (ϕ) for each pixel over the upwind footprint source area (Ω_Π),

$$F_{region} = \iint_{\Omega_P} F(x,y)\phi(x,y)dxdy. \qquad (11)$$

The surface CO_2 flux F(x,y) can be any component of carbon fluxes, i.e., GPP or R. In this study, we focus on GPP. The spatially explicit BEPS model was used to simulate GPP at 1 km resolution over the concentration footprint area of the SOBS tower. The daily concentration footprint function (ϕ) for each pixel (same size as BEPS) was simulated using SAFE.

3.4. Method for Deriving Local GPP From EC Measurements

[25] The surface flux was calculated as the sum of the eddy flux, measured at 25 m, and the rate of change of storage in the air column below the flux measurement level. The surface CO_2 flux provides a direct measurement of the net ecosystem exchange (F_{NEE})—the net exchange rate of CO_2 between the ecosystem and the atmosphere. Following *Barr et al.* [2004], two adjustments were applied to F_{NEE}: the nighttime F_{NEE} data are excluded at low u_* (here, $u_* <$ 0.35 m s^{-1}) and an energy-balance-closure adjustment is applied by dividing the measured F_{NEE} by the fractional energy balance closure (here, 89%), calculated as the ratio of the sum of the sensible and latent heat fluxes to the available energy flux. F_{NEE} provides a direct measure of the net ecosystem production ($F_{\mathrm{NEP}} = -F_{\mathrm{NEE}}$). At local scale (i.e., EC flux footprint area), F_{NEP} results as the difference between carbon gains by GPP and carbon losses by R (i.e., F_{NEP} = GPP − R). Positive values of F_{NEP} correspond to CO_2 uptake by the ecosystem.

[26] R and GPP were derived from F_{NEP} measurements. The measured R was estimated as $R = -F_{\mathrm{NEP}}$ during periods when GPP was known to be zero, i.e., growing-season nighttime F_{NEP} measurements and non-growing-season (periods when both air (T_a) and 2-cm soil (T_s) temperatures were lower than 0°C). GPP was obtained from measured F_{NEP} and estimated daytime R_d as GPP = $F_{\mathrm{NEP}} + R_d$. The core of this methodology was to first derive simple annual empirical relationships (for example, $R_d = f(T_S)$) from measured data. R_d values were estimated from an empirical logistic equation (fitted to the measured R values from the entire year [*Barr et al.*, 2004],

$$R_d = f(T_s, t) = \frac{r_t(t)r_1}{1 + \exp(r_2(r_3 - T_s))}, \qquad (12)$$

where T_S is measured at the 5-cm depth; r_1, r_2, and r_3 are the empirical parameters, held constant over the year; and $r_t(t)$ is a time-varying parameter. The values of $r_t(t)$ were estimated within a 100-point moving window as the slope of a linear regression (forced through zero) of the modeled R estimates from (equation (12)) versus measured R.

4. Results

4.1. Atmospheric Diffusion and Ecosystem Modeling

[27] A critical step in our methodology of extracting the photosynthesis signal from the CO_2 record is to ensure that atmospheric diffusion is simulated with a reasonable accuracy. Although the integrated ecosystem-boundary layer model has been shown to perform well in the previous studies [*Chen et al.*, 2004; *B. Chen et al.*, 2005, 2006a, 2006b; *J. M. Chen et al.*, 2007], model validation of simulated CO_2 mixing ratio against measurements at this

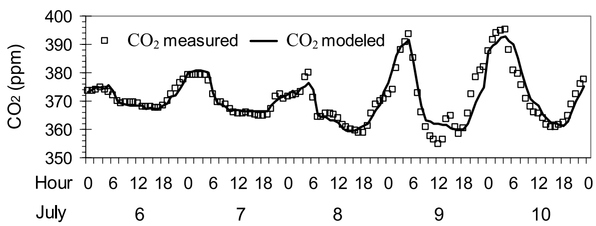

Figure 3. Comparison of measured (symbols) and modeled (solid line) CO_2 mixing ratios for 6–10 July 2003.

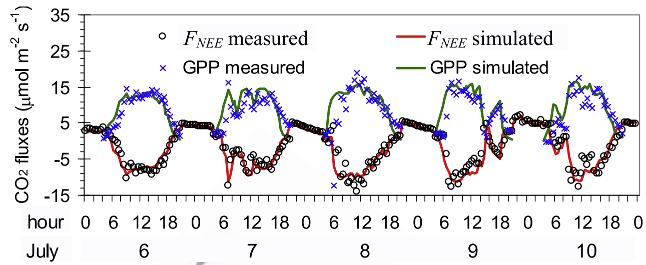

Figure 4. Comparison of the EC-measured half-hourly net ecosystem exchange (F_{NEE}) and EC flux derived GPP with BEPS simulated half-hourly net ecosystem exchange (F_{NEE}) and GPP for 6–10 July 2003.

SOBS tower was also made in this study. Figure 3 provides examples of the simulated CO_2 mixing ratios in comparison with observed values for five consecutive days in July 2003. The simulated curves generally followed the observed values closely, even though the simulation was made with a simple one-dimensional model. The simulated curves were generally smoother than the observed values because of the assumption of horizontal homogeneity used in the 1-D model. There were synoptic events (frontal systems) causing abrupt changes in CO_2 concentration, and simulated values from the 1-D model had the largest departure from measurements under these circumstances (e.g., 9 July, as shown in Figure 3). Similar simulation results were obtained for all days in 2003, and the results were summarized in Table 1 in terms of regression statistics between modeled and observed CO_2 concentrations. The r^2 value increases and the root mean square error (RMSE) decreases as the modeled hourly values are averaged for daily and 10-d periods, suggesting that the 1-D model can generally capture the underlying ecosystem variability for regional carbon balance estimation.

[28] To ensure that atmospheric diffusion is simulated with an acceptable accuracy for our purpose of using a CO_2 record for deriving ecosystem information, we should also have the first order estimate of the CO_2 flux to and from the underlying the surface. Figure 4 shows comparison of the EC-measured F_{NEE} and GPP derived from EC flux measurements with simulated F_{NEE} and GPP for the same period as shown in Figure 3. The model simulations generally had good agreement with observations.

[29] After gaining confidence in modeling the atmospheric diffusion and ecosystem metabolism, we applied the methodology illustrated in section 3.2.2 and *J. M. Chen et al.* [2007] to the entire record of CO_2 in 2003. Daily GPP values were computed from the hourly CO_2 concentration for the whole year (see section 4.4).

Table 1. Statistics for the Regression Between Modeled and Observed CO_2 Concentrations on the SOBS Tower for Hourly, Daily, and 10-d Mean Values[a]

	r^2	RMSE (ppm)	Sample Size (n)
Hourly	0.67	4.8	6910
Daily	0.73	2.3	291
10 d	0.87	2.1	36

[a]The r^2 is the linear regression coefficient, and RMSE is the root mean square error, $= \sqrt{\frac{1}{n}\sum_{i=1}^{n}[C_{\mathrm{mod}}(i) - C_{\mathrm{obs}}(i)]^2}$.

4.2. Estimates of Daily Concentration Footprint

[30] SAFE was applied to the SOBS tower for 2003. To be compatible with BEPS, the grid size in SAFE was set to be 1 km × 1 km. The calculated footprints are shown in Figure 5 for four arbitrary days in 2003. The parameters for characterizing the daily mean wind and atmospheric stability for these 4 d are listed in Table 2. The footprint peak was about 10 km upwind of the tower, and the upwind tail within the cutoff point extended up to 250–350 km depending on weather conditions (Figure 5a). The crosswind distribution followed the assumed Gaussian distribution, but the decline rates from the peak isopleth depended on the atmospheric stability and the standard deviation of the lateral spread (Figure 5b). Different days had different footprints (Figures 6a and 6b) as the air flowed from different directions with different widths of dispersion. The northwest winds contributed the most to the annual footprint for the SOBS tower in 2003, while northeast winds contributed the least (Figure 7).

4.3. Simulated GPP Field at 1 km Resolution

[31] The spatially explicit BEPS model was used for simulating the GPP over the concentration footprint area of the SOBS tower. Values of the daily total GPP at 1 km resolution for 11 and 24 August were shown in Figures 6c and 6d, as examples. The differences between these 2 d were apparent. On the basis of the simulated daily GPP and daily weighted concentration footprint, we calculated the daily regional GPP values that influence the concentration measurements at the tower using equation (11) for the whole year (Figure 9).

4.4. Comparison of GPP Estimates

[32] In order to test the performance of BEPS, model parameters were not "tuned" to obtain a better match with the tower observations, and the land surface inputs were derived from remote sensing images instead of using the measurements. As shown in Figure 8, the simulated daily GPP in the 1 km pixel containing the SOBS tower generally

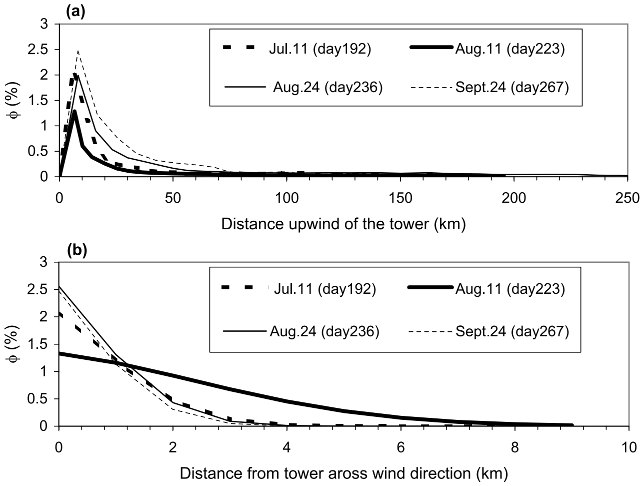

Figure 5. Simulated concentration footprint cross sections for four arbitrary days in 2003. (a) Along the wind direction and (b) across the wind direction from center line of the mean flow. The parameters for characterizing the daily mean wind and atmospheric stability are listed in Table 2.

followed the EC flux derived GPP (r^2 = 0.76) well because they represent the similar local source area (EC flux footprint area: about 1 km^2 surrounding the tower), but the model tends to underestimate the measured GPP in the middle growing season. Estimates of GPP using the PBL-budget method are likely representative of a regional scale owing to the large source area that affects the mixing ratio (concentration footprint area: about 10^3–10^5 km^2). The source areas are the same in the PBL-budgeting (method 1) and the concentration-footprint-integrating (method 2) approaches. The estimates of daily GPP by these two approaches were compared in Figure 9. The PBL-budgeted estimates were in good agreement with the concentration-footprint-integrated estimates (slope = 0.99; r^2 = 0.89). In order to test these methods to infer the regional GPP from mixing ratio measurements, we also compared the estimates of regional GPP with EC flux derived GPP although their source areas are different. Regression analysis revealed that they were highly correlated but concentration-derived daily GPP only reached about 80% of the magnitudes of EC flux derived daily GPP (Figure 10). The seasonal patterns of the weekly averages of GPP estimated by these four approaches (at both local and regional scales) were quite similar although the spatial scales represented by these four sets of estimates were very different (Figure 11). Similar to regression analysis at daily time steps (Figure 10), we also see from Figure 11 that the regional GPP estimates were consistently much smaller than the local GPP for all days in 2003. This is consistent with characteristics of the source areas (different land cover types) represented by these two quantities. The EC flux footprint area (local GPP) is dominated by a black spruce forest while the concentration footprint areas (regional GPP) include forest, shrub, grass, agriculture crop fields and open water bodies, all of which are likely to be less productive. Seasonal budgets of GPP estimates were summarized in Table 3 and Figure 12. The estimates of annual GPP were about 819–847 g C m^{-2} for the smaller area surrounding the tower and 649–664 g C m^{-2} for the region around the tower, respectively. The differences in GPP estimates by different methods for the similar spatial scales were within 4%. The regional estimates were about 20–25% lower than the local estimates and most of the differences occurred during the early to middle growing season (i.e., May to June, Figure 12).

5. Discussion

[33] This study makes use of measurements of the high-frequency CO_2 mixing ratio on a short tower to estimate the net CO_2 exchange at daily or longer timescales. The PBL dynamics naturally integrate the effects of land ecosystems on the atmosphere at a regional scale. Because of the convective boundary layer (CBL) dynamics, the influence of the inhomogeneous surface on the atmospheric CO_2 is smoothed, and the evolution of atmospheric CO_2 with time in a day represents the integrated influence of the surface flux over the concentration footprint. The surface area that influences the PBL for 1 d is estimated to be about 10^4 km^2 [*Raupach et al.*, 1992]. Mixing within the CBL occurs rapidly (~15 min) relative to the timescale for substantial changes in surface fluxes (~1 h except near sunrise and sunset). This allows simple mass-balance approaches to relate average CBL concentrations to the surface flux [*Styles et al.*, 2002]. The daily GPP extracted from hourly CO_2 concentration measurements (method 1) should represent the upwind area of the tower in the mean wind direction on a given day. The daily concentration footprint area was estimated to be around 10^3–10^4 km^2, smaller than 10^4–10^5 km^2 for multiple days [*Gloor et al.*, 2001; *Lin et al.*, 2004]. Though it is difficult to separate the near-field and the far-field effects on the estimated daily GPP using our methodology, the far-field effect on daily GPP estimation is quite small. We therefore expect the biases in estimated daily GPP by neglecting the change in background atmospheric CO_2 in our one-dimensional ecosystem-boundary layer model are not significant.

[34] Moreover, satellite data provide independent information on the spatial and phenological variations of GPP using an ecosystem model such as BEPS. Given a reasonable estimate of the actual footprint under certain micrometeorological conditions and a simulation of the surface flux field by BEPS based on remote sensing, we can calculate the daily regional GPP values that influence the

Table 2. Parameters for Characterizing the Wind and Atmospheric Stability for the Four Arbitrary Days as Shown in Figure 5[a]

	u (m s^{-1})	σ_v (m s^{-1})	σ_d (degrees)	u_* (m s^{-1})	$1/L$ ($\times10^{-3}$) (m^{-1})	R_b
11 Jul	3.3	1.8	20.4	0.48	−9.9	0.15
11 Aug	3.7	2.6	25.1	0.53	−30.8	0.08
24 Aug	5.2	2.2	14.8	0.74	−1.6	0.05
24 Sep	3.9	2.3	15.7	0.54	−3.2	0.05

[a]Where u is the wind velocity, σ_v is the standard deviation of lateral wind velocity fluctuations, σ_d is the standard deviation of lateral wind directions, u_* is the friction wind speed, $1/L$ is the reciprocal of Obukhov length, and R_b is the bulk Richardson number.

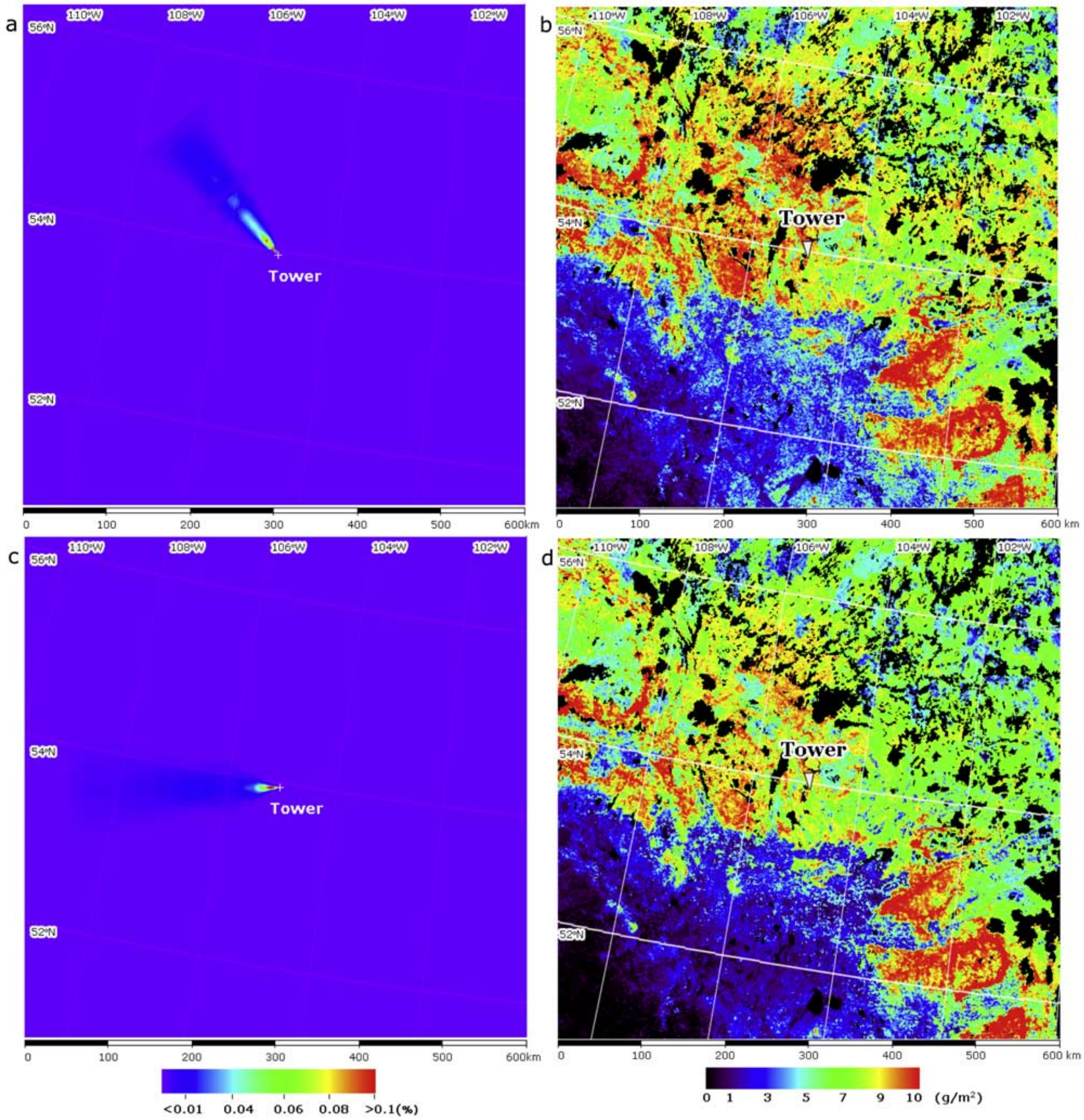

Figure 6. Simulated footprint and gross primary productivity (GPP) maps at 1 km resolution on two arbitrary days. (a) The footprint and (b) GPP maps for 11 August 2003. (c, d) The corresponding maps for 24 August 2003.

concentration measurements using equation (11) (method 2). This is an effective method to retrieve the regional carbon flux information which is "seen" by the concentration sensor on the tower.

[35] The PBL carbon budget (i.e., concentration-derived) method uses a one-dimensional ecosystem-boundary layer model. By "turning off" the modeled GPP and estimating the actual GPP through PBL budgeting from the accumulated increase in CO_2 concentration, modeled after GPP is "turned off", from the observed CO_2 concentration at sunset, we greatly reduce the error due to surface heterogeneity. However, this methodology does not tell which the source area the concentration-derived GPP represents. As the air flows from different directions over different underlying surfaces, large day-to-day variations are expected even though the micrometeorological conditions are similar. The combination of concentration footprint estimation with remote sensing based GPP estimation provides an opportu-

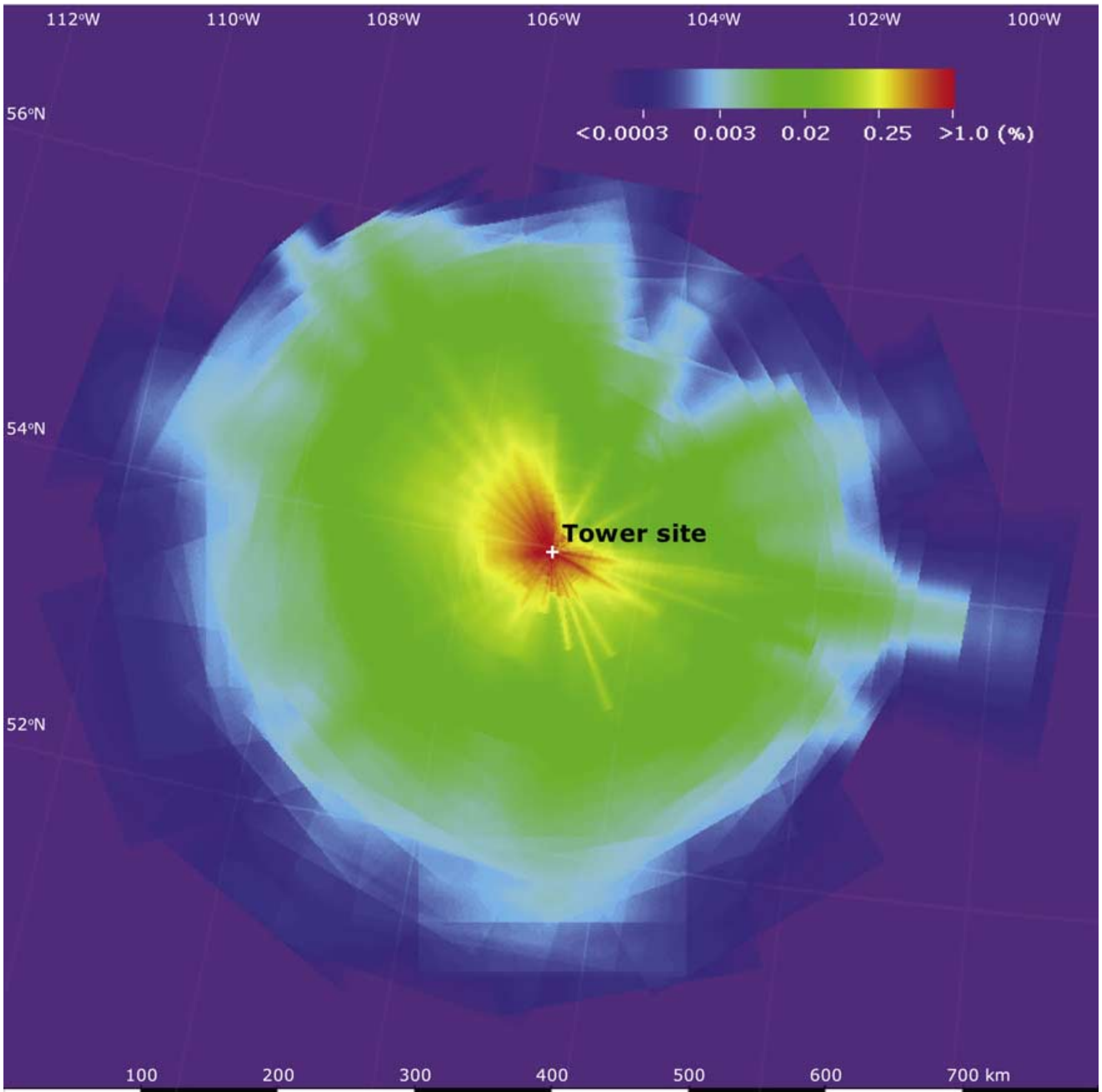

Figure 7. Annual concentration footprint for the SOBS tower for 2003.

nity to evaluate the reliability of the concentration-derived GPP as it explicitly considers the source areas for the concentration measurements. The significance of concentration-derived flux information is its large concentration footprint consisting of many cover types of different vegetation densities, and so far there has been no other ways to validate carbon cycle information derived from atmospheric CO_2 mixing ratio measurements.

[36] In this study, these two independent regional GPP estimates showed close agreement. However, it must be realized that it is still possible that both of them have similar biases, i.e., simultaneously overestimated or underestimated. We assume the MBL reference CO_2 as a substitute for background value (free tropospheric value) for the two methods. The departures of free tropospheric concentrations from MBL reference over the continent was reported to be ~3 ppm in some regions, with an averaging value of ~1–2 ppm according to the CO_2 Budget and Rectification Airborne study (COBRA) measurements [*Gerbig et al.*, 2003; *Lin et al.*, 2004, 2006]. Such systematic departures can be explained in large part by advection from different latitudes and by time lags in vertical propagation of concentration changes at the surface, within the MBL, to the free troposphere [*Gerbig et al.*, 2003]. A typical vertical CO_2 gradient (PBL-free troposphere) was lager than 10 ppm during summer growing season in the research area. Suppose the difference in CO_2 concentration between free troposphere and MBL is 1.5 ppm in summer, the potential errors in estimated regional GPP by the presented methods could be less than 5–10% from substituting the MBL reference.

[37] It is therefore also paramount that the ecosystem model used to derive the flux field for footprint integration is validated at some locations within and near the footprint area. Our confidence in both the concentration-derived and footprint-integrated regional GPP estimates is gained from the fact that the BEPS model used for GPP mapping agreed

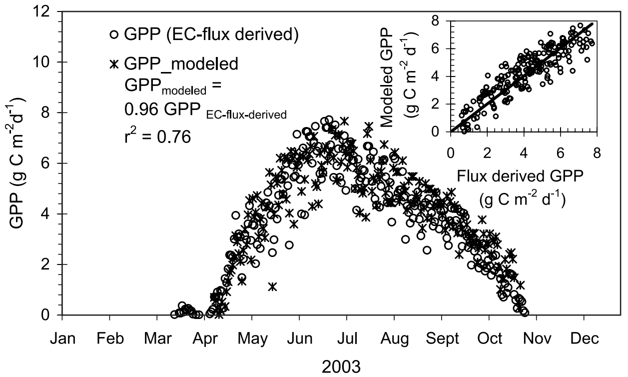

Figure 8. Comparison of BEPS simulated daily GPP of the 1 × 1 km pixel which contains the SOBS tower with that derived from EC flux measurements. The inset shows the linear regression between these two GPP estimates.

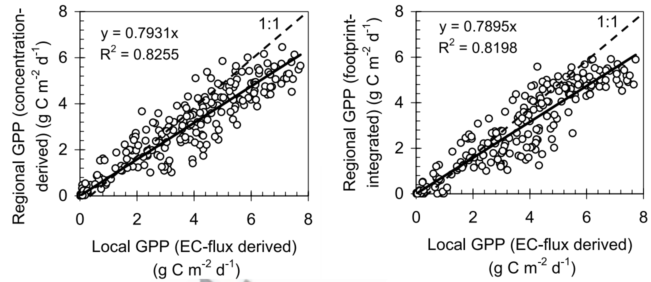

Figure 10. Comparisons of concentration-derived and footprint-integrated regional GPP with EC-derived local GPP on a daily time basis.

well with EC-derived GPP at a given site within the flux footprint. This eases our concern about possible significant model biases. The comparisons of these regional GPP estimates with EC flux measurements showed that they had similar seasonal patterns but the regional estimates were consistently smaller than local EC-derived GPP throughout the growing season in 2003. The annual differences were about 20–25%. The spatial representations of these two GPP estimates are very different: the EC footprint is the relatively homogeneous old black spruce while the concentration footprint is covered by boreal needle evergreen and deciduous broadleaf forests, shrub land, grass land, crop land, and lakes. The discrepancies between these two GPP estimates reflect the differences in the underlying land surface. From the GPP maps modeled by BEPS we have quantitatively evaluated that GPP values for nonforest types are much lower than that of the SOBS site, and this is consistent with the fact that both concentration-derived and concentration-footprint-integrated GPP values are considerably lower than the EC measurements. This large difference indicates the importance of considering the surface heterogeneity when we attempt to extrapolate site measurements to the region. It is encouraging to see that atmospheric CO_2 concentration data can be used effectively for this upscaling purpose.

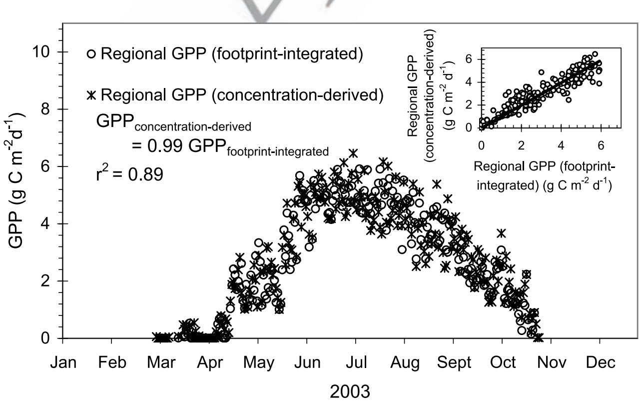

Figure 9. Comparison of concentration-derived regional GPP with footprint-integrated regional GPP on a daily time basis for 2003. The inset shows the linear regression between these two GPP estimates.

[38] There are three main assumptions made in obtaining the concentration-derived GPP during daytime [see *J. M. Chen et al.*, 2007]. In using this methodology, caution should be taken against potential errors due to (1) conditions when the PBL is not well mixed during the day, (2) highly heterogeneous atmospheric conditions such as those caused by water-land interfaces and complex terrain, and (3) diurnally variable anthropogenic CO_2 sources. At nighttime, the atmosphere is highly stratified, and the similarity of uniform vertical mixing within the PBL is no longer valid. This methodology is therefore not applicable to extracting nighttime F_{NEE} or R.

[39] CO_2 concentration data can be possibly used to infer F_{NEE} and R by tuning an ecosystem model when the atmospheric diffusion during daytime and nighttime is reasonably well simulated [*B. Chen et al.*, 2006a, 2006b]. It is feasible to retrieve R and F_{NEE} at regional scale by combining concentration footprint modeling with ecological modeling based on remote sensing. Simple PBL budget analysis making use of the differences in the CO_2 mixing ratio between the surface layer and the free troposphere (C_{FT}) to compute F_{NEE} on a monthly basis has been explored [*Helliker et al.*, 2004; *Bakwin et al.*, 2004; *Lai et al.*, 2006]. All of them used the marine boundary layer data

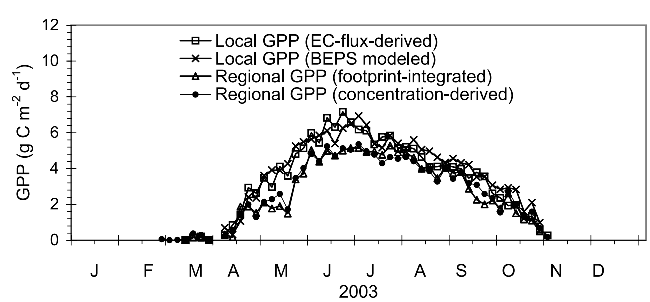

Figure 11. Mean 5-d GPP estimated by four different approaches based on EC flux and CO_2 concentration measurements at the SOBS site, 2003.

Table 3. Monthly and Annual GPP Estimates From These Four Approaches for the SOBS Tower, 2003[a]

Scales	Methods	Mar	Apr	May	Jun	Jul	Aug	Sep	Oct	Annual
Local	EC flux derived	1.8	40.4	126.4	192.3	177.0	137.1	102.8	40.8	818.6
	BEPS modeled		30.5	138.4	179.7	180.3	150.2	110.7	56.9	846.7
Regional	Footprint integrated	1.2	26.7	77.7	145.5	155.5	127.9	76.6	38.1	649.2
	Concentration derived	3.3	27.3	86.5	145.7	149.1	120.0	86.3	46.0	664.2

[a]Units are g C m^{-2}.

to estimate C_{FT}. The CO_2 entrainment at the CBL top is critical to this methodology. *Helliker et al.* [2004] estimated the vertical transfer by analyzing the budget of water vapor in the CBL with the surface flux of water vapor measured by EC methods, while the others used National Centre for Environmental Prediction (NECP) reanalysis data for the same purpose. These simple budget analyses have been shown to be successful on monthly and seasonal bases, but biases and uncertainties are still considerable [*Bakwin et al.*, 2004; *Lai et al.*, 2006; *Crevoisier et al.*, 2006]. In comparison with this methodology for net carbon exchange, our methods of deriving GPP during the daytime and *R* during both nighttime and daytime has the advantage of inferring carbon components necessary for model validation and ecosystem parameter optimization for regional (i.e., $\sim 10^5$ km^2) applications.

6. Conclusions

[40] To quantify regional carbon fluxes using high-frequency CO_2 concentration measurements, we have explored and compared two independent methods: (1) PBL carbon budgeting using an integrated ecosystem-boundary model (i.e., BEPS-VDS), and (2) remote sensing based concentration footprint integration using a spatially explicit ecosystem model (BEPS) driven by remote sensing inputs and a new concentration footprint model (SAFE). The following three conclusions were drawn from the application of these methodologies to the SOBS tower in 2003 after the validation of BEPS using EC measurements at the site:

[41] 1. Both concentration-derived and footprint-integrated GPP values agreed well and the model used for GPP estimation within the footprint agreed well with EC measurements, suggesting that these two methods are both useful for obtaining regional carbon flux information.

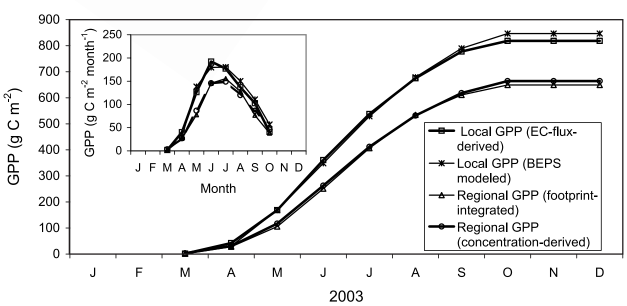

Figure 12. Annual cumulations of four GPP estimates for the SOBS site and the region around the site, 2003. The inset shows seasonal courses of the monthly total GPP.

[42] 2. These two methods have advantages and disadvantages: the concentration-derived GPP does not indicate the size of the source area, while the remote sensing based footprint integrating method quantifies the source area. The former is vulnerable to PBL height simulations and requires some assumptions (see section 5), while the latter is sensitive to model parameterization in both the ecosystem model (i.e., BEPS) and footprint model (SAFE). To use the two methods as a pair is a practical and effective means to derive regional carbon fluxes (i.e., GPP in this study) with high temporal resolution (i.e., at daily time steps). Combining these two methods has an obvious advantage over those approaches for net carbon flux [e.g., *Helliker et al.*, 2004; *Bakwin et al.*, 2004].

[43] 3. The influence of the inhomogeneous surface over the footprint on the atmospheric CO_2 is smoothed by the CBL dynamics, and the evolution of atmospheric CO_2 with time during 24 h represents the integrated influence of the surface flux at a regional scale (10^2–10^4 km^2). This study shows that atmospheric CO_2 concentration data can be used effectively to extrapolate site CO_2 flux measurements to a region.

[44] **Acknowledgments.** This work is supported by the Canadian Foundation for Climate and Atmospheric Sciences as part of the Fluxnet Canada Research Network. We would like to acknowledge Douglas Worthy at Atmospheric Science and Technology Directorate, Environment Canada, for the measurements of the CO_2 concentration.

References

Arain, A., T. A. Black, A. G. Barr, P. G. Jarvis, J. M. Massheder, D. L. Verseghy, and Z. Nesic (2002), Effects of seasonal and interannual climate variability on net ecosystem productivity of boreal deciduous and conifer forests, *Can. J. For. Res.*, *32*, 878–891.

Bakwin, P. S., P. P. Tans, D. F. Hurst, and C. Zhao (1998), Measurements of carbon dioxide on very tall towers: Results of the NOAA/CMDL program, *Tellus, Ser. B*, *50*, 401–415.

Bakwin, P. S., K. J. Davis, C. Yi, S. C. Wofsy, J. W. Munger, L. Haszpra, and Z. Barcza (2004), Regional carbon dioxide fluxes from mixing ratio data, *Tellus, Ser. B*, *56*, 301–311.

Barr, A. G., T. A. Black, E. H. Hogg, N. Kljun, K. Morgenstern, and Z. Nesic (2004), Inter-annual variability in the leaf area index of a boreal aspen–hazelnut forest in relation to net ecosystem production, *Agric. For. Meteorol.*, *126*, 237–255.

Black, T. A., G. den Hartog, H. Neumann, P. Blanken, P. Yang, Z. Nesic, S. Chen, C. Russel, P. Voroney, and R. Stabeler (1996), Annual cycles of CO2 and water vapor fluxes above and within a Boreal aspen stand, *Global Change Biol.*, *2*, 219–229.

Baldocchi, D. D., et al. (2001), Fluxnet: A new tool to study the temporal and spatial variability of ecosystem-scale carbon dioxide, water vapor, and energy flux densities, *Bull. Am. Meteorol. Soc.*, *82*, 2415–2434.

Bousquet, P., P. Ciais, P. Peylin, M. Ramonet, and P. Monfray (1999), Inverse modeling of annual atmospheric CO_2 sources and sinks: 1. Method and control inversion, *J. Geophys. Res.*, *104*, 26,161–26,178.

Chen, B., and J. M. Chen (2007), Diurnal, seasonal and inter-annual variability of carbon isotope discrimination at the canopy level in response to environmental factors in a boreal forest ecosystem, *Plant Cell Environ.*, *30*, 1223–1239.

Chen, B., J. M. Chen, J. Liu, D. Chan, K. Higuchi, and A. Shashkov (2004), A vertical diffusion scheme to estimate the atmospheric rectifier effect, *J. Geophys. Res.*, *109*, D04306, doi:10.1029/2003JD003925.

Chen, B., J. M. Chen, and D. Worthy (2005), Interannual variability in the atmospheric CO_2 rectification over a boreal forest region, *J. Geophys. Res.*, *110*, D16301, doi:10.1029/2004JD005546.

Chen, B., J. M. Chen, P. P. Tans, and L. Huang (2006a), Modeling dynamics of stable carbon isotopic exchange between a boreal ecosystem and the atmosphere, *Global Change Biol.*, *12*, 1842–1867.

Chen, B., J. M. Chen, L. Huang, and P. P. Tans (2006b), Simulating dynamics of $\delta^{13}C$ of CO_2 in the planetary boundary layer over a boreal forest region: Covariation between surface fluxes and atmospheric mixing, *Tellus, Ser. B*, *58*, 537–549.

Chen, B., J. M. Chen, M. Gang, C.-W. Yuen, K. Higuchi, and D. Chan (2007), Modeling and scaling coupled energy, water, and carbon fluxes based on remote sensing: An application to Canada's landmass, *J. Hydrometeorol.*, *8*, 123–143.

Chen, J. M., J. Liu, J. Cihlar, and M. L. Guolden (1999), Daily canopy photosynthesis model through temporal and spatial scaling for remote sensing applications, *Ecol. Modell.*, *124*, 99–119.

Chen, J. M., et al. (2002), Validation of Canada-wide leaf area index maps using ground measurements and high and moderate resolution satellite imagery, *Remote Sens. Environ.*, *80*, 165–184.

Chen, J. M., C. H. Menges, and S. G. Leblanc (2005), Global mapping of foliage clumping index using multi-angular satellite data, *Remote Sens. Environ.*, *97*, 447–457.

Chen, J. M., B. Chen, K. Higuchi, J. Liu, D. Chan, D. Worthy, P. Tans, and T. A. Black (2006), Boreal ecosystems sequestered more carbon in warmer years, *Geophys. Res. Lett.*, *33*, L10803, doi:10.1029/2006GL025919.

Chen, J. M., B. Chen, and P. Tans (2007), Deriving daily carbon fluxes from hourly CO2 mixing ratios measured on the WLEF tall tower: An upscaling methodology, *J. Geophys. Res.*, *112*, G01015, doi:10.1029/2006JG000280.

Crevoisier, C., M. Gloor, E. Gloaguen, L. W. Horowitz, J. Sarmiento, C. Sweeney, and P. Tans (2006), A direct carbon budgeting approach to infer carbon sources and sinks: Design and synthetic application to complement the NACP observation network, *Tellus, Ser. B*, *58*, 366–375.

Enting, I. G., C. M. Trudinger, and R. J. Francey (1995), A synthesis inversion of the concentration and $\delta^{13}C$ of atmospheric CO_2, *Tellus, Ser. B*, *47*, 35–52.

Fan, S., M. Gloor, J. Mahlman, S. Pacala, J. Sarmiento, T. Takahashi, and P. Hans (1998), A large terrestrial carbon sink in North America implied by atmospheric and oceanic carbon dioxide data and models, *Science*, *282*, 442–446.

Friedlingstein, P., J. L. Dufresne, P. M. Cox, and P. Rayner (2003), How positive is the feedback between climate change and the carbon cycle?, *Tellus, Ser. B*, *55*, 692–700.

Fung, I. Y., S. C. Doney, K. Lindsay, and J. John (2005), Evolution of carbon sinks in a changing climate, *Proc. Nat. Acad. Sci.*, *102*, 11,201–11,206.

Fung, I. Y., K. Prentice, E. Matthews, J. Lerner, and G. Russell (1983), Three-dimensional tracer model study of atmospheric CO_2: Response to seasonal exchanges with the terrestrial biosphere, *J. Geophys. Res.*, *88*, 1281–1294.

Gerbig, C., J. C. Lin, S. C. Wofsy, B. C. Daube, A. E. Andrews, B. B. Stephens, P. S. Bakwin, and C. A. Grainger (2003), Toward constraining regional-scale fluxes of CO_2 with atmospheric observations over a continent: 1. Observed spatial variability from airborne platforms, *J. Geophys. Res.*, *108*(D24), 4756, doi:10.1029/2002JD003018.

GLOBALVIEW-CO_2 (2005), *Cooperative Atmospheric Data Integration Project: Carbon Dioxide* [CD-ROM], NOAA Clim. Monit. and Diag. Lab., Boulder, Colo. (Available via anonymous FTP to ftp.cmdl.noaa.gov, Path: ccg/co2/GLOBALVIEW)

Gloor, M., S. M. Fan, S. Pacala, J. Sarmiento, and M. Ramonet (1999), A model-based evaluation of inversions of atmospheric transport, using annual mean mixing ratios, as a tool to monitor fluxes of nonreactive trace substances like CO_2 on a continental scale, *J. Geophys. Res.*, *104*, 14,245–14,260.

Gloor, M., P. Bakwin, D. Hurst, L. Lock, R. Draxler, and P. Tans (2001), What is the concentration footprint of a tall tower?, *J. Geophys. Res.*, *106*, 17,831–17,840.

Griffis, T. J., T. A. Black, K. Morgenstern, A. G. Barr, Z. Nesic, G. B. Drewitt, and D. Gaumont-Guay (2003), Ecophysiological controls on the carbon balances of three southern boreal forests, *Agric. For. Meteorol.*, *125*, 207–223.

Gurney, K. R., et al. (2002), Towards robust regional estimates of CO_2 sources and sinks using atmospheric transport models, *Nature*, *415*, 626–630.

Helliker, B. R., J. A. Berry, A. K. Betts, P. S. Bakwin, K. J. Davis, A. S. Denning, J. R. Ehleringer, J. B. Miller, M. P. Butler, and D. M. Ricciuto (2004), Estimates of net CO_2 flux by application of equilibrium boundary layer concepts to CO_2 and water vapor measurements from a tall tower, *J. Geophys. Res.*, *109*, D20106, doi:10.1029/2004JD004532.

Horst, T. W., and J. C. Weil (1992), Footprint estimation for scalar flux measurements in the atmospheric surface layer, *Boundary Layer Meteorol.*, *59*, 279–296.

Jarvis, P. G., J. M. Massheder, S. E. Hale, J. B. Moncrieff, M. Rayment, and S. L. Scott (1997), Seasonal variation of carbon dioxide, water and energy exchanges of a boreal black spruce forest, *J. Geophys. Res.*, *102*, 28,953–28,966.

Ju, W., J. M. Chen, T. A. Black, A. Barr, J. Liu, and B. Chen (2006), Modeling coupled water and carbon fluxes in a boreal aspen forest, *Agric. For. Meteorol.*, *140*, 136–151.

Kljun, N., R. Kormann, M. W. Rotach, and F. X. Meixer (2003), Comparison of the Lagrangian footprint model LPDM-B with an analytical footprint model, *Boundary Layer Meteorol.*, *106*, 349–355.

Kljun, N., T. A. Black, T. J. Griffis, A. G. Barr, D. Gaumont-Guay, K. Morgenstern, J. H. McCaughey, and Z. Nesic (2006), Response of net ecosystem productivity of three boreal forest stands to drought, *Ecosystems*, *9*, 1128–1144.

Lacelle, B. (1997), Canada's soil organic carbon database, in *Soil Processes and the Carbon Cycle*, edited by R. Lal et al., pp. 93–102, CRC Press, New York.

Lai, C.-T., A. J. Schauer, C. Owensby, J. M. Ham, B. Helliker, P. Tans, and J. R. Ehleringer (2006), Regional CO_2 fluxes inferred from mixing ratio measurements: estimates from flask air samples in central Kansas, USA, *Tellus, Ser. B*, *58*, 523–536.

Law, B. E., et al. (2002), Environmental controls over carbon dioxide and water vapor exchange of terrestrial vegetation, *Agric. For. Meteorol.*, *113*, 97–120, doi:10.1016/S0168-1923(02)00104-1.

Levy, P. E., A. Grelle, A. Lindroth, M. Mölder, P. G. Jarvis, B. Kruijt, and J. B. Moncrieff (1999), Regional-scale CO_2 fluxes over central Sweden by a boundary layer budget method, *Agric. For. Meteorol.*, *98/99*, 169–180.

Lin, J. C., C. Gerbig, S. C. Wofsy, A. E. Andrews, B. C. Daube, C. A. Grainger, B. B. Stephens, P. S. Bakwin, and D. Y. Hollinger (2004), Measuring fluxes of trace gases at regional scales by Lagrangian observations: Application to the CO_2 Budget and Rectification Airborne (COBRA) study, *J. Geophys. Res.*, *109*, D15304, doi:10.1029/2004JD004754.

Lin, J. C., C. Gerbig, S. C. Wofsy, B. C. Daube, D. M. Matross, V. Y. Chow, E. Gottlieb, A. E. Andrews, M. Pathmathevan, and J. W. Munger (2006), What have we learned from intensive atmospheric sampling field programs of CO_2?, *Tellus, Ser. B*, *58*, 331–343.

Liu, J., J. M. Chen, J. Cihlar, and W. Chen (1999), Net primary productivity distribution in BOREAS region from a process model using satellite and surface data, *J. Geophys. Res.*, *104*, 27,735–27,754.

Liu, J., J. M. Chen, J. Cihlar, and W. Chen (2002), Net primary productivity mapped for Canada at 1-km resolution, *Global Ecol. Biogeogr.*, *11*, 115–129.

Masarie, K. A., and P. P. Tans (1995), Extension and integration of atmospheric carbon dioxide data into a globally consistent measurement record, *J. Geophys. Res.*, *100*, 593–1610.

Matross, D., A. Andrews, and M. Pathmathevan (2006), Estimating regional carbon exchange in New England and Quebec by combining atmospheric, ground-based and satellite data, *Tellus, Ser. B*, *58*, 344–358.

Moeng, C. H., and J. C. Wyngaard (1989), Evaluation of turbulent transport and dissipation closures in 2nd-order modeling, *J. Atmos. Sci.*, *46*, 2311–2330.

Pasquill, F. (1974), *Atmospheric Diffusion*, 2nd ed., 437 pp., J. Wiley, New York.

Potosnak, M. J., S. C. Wofsy, A. S. Denning, T. J. Conway, J. W. Munger, and D. H. Barnes (1999), Influence of biotic exchange and combustion sources on atmospheric CO_2 concentration in New England from observations at a forest flux tower, *J. Geophys. Res.*, *104*, 9561–9569.

Raupach, M. R., O. T. Denmead, and F. X. Dunin (1992), Challenges in linking atmospheric CO_2 concentrations to fluxes at local and regional scales, *Aust. J. Bot.*, *40*, 697–716.

Rodenbeck, C., S. Houweling, M. Gloor, and M. Heimann (2003), CO_2 flux history 1982–2001 inferred from atmospheric data using a global inversion of atmospheric transport, *Atmos. Chem. Phys.*, *3*, 1919–1964.

Schmid, H. P. (1994), Source areas for scalar and scalar fluxes, *Boundary Layer Meteorol.*, *67*, 293–318.

Schut, P., J. Shields, C. Tarnocai, D. Coote, and I. Marshall (1994), Soil landscapes of Canada: An environmental reporting tool, paper presented at Canadian Conference on GIS, Agriculture Canada, Ottawa, Canada, 6–10 June.

Sellers, P. J., et al. (1997), BOREAS in 1997: Experiment overview, scientific results, and future directions, *J. Geophys. Res.*, *102*, 28,731–28,769.

Shields, J. A., C. Tarnocai, K. W. G. Valentine, and K. B. MacDonald (1991), *Soil Landscapes of Canada: Procedures Manual and User's Hand Book*, *Agric. Can. Publ. 1868/E*, Agric. Can., Ottawa, Canada.

Styles, J. M., J. Lloyd, D. Zolotoukhine, K. A. Lawton, N. Tchebakova, R. J. Francey, A. Arneth, D. Salamakho, O. Kolle, and E.-D. Schulze (2002), Estimates of regional surface carbon dioxide exchange and carbon and oxygen isotope discrimination during photosynthesis from concentration profiles in the atmospheric boundary layer, *Tellus, Ser. B*, *54*, 768–783.

Tans, P. P., I. Y. Fung, and T. Takahashi (1990), Observational constraints on the global atmospheric CO_2 budget, *Science*, *247*, 1431–1438.

van Ulden, A. P. (1978), Simple estimates for vertical diffusion from sources near the ground, *Atmos. Environ.*, *12*, 2125–2129.

Wyngaard, J. C., and R. A. Brost (1984), Top-down and bottom-up diffusion of a scalar in the convective boundary layer, *J. Atmos. Sci.*, *41*, 102–112.

Zhang, D., and R. Anthes (1982), A high-resolution model of the planetary boundary layer-sensitivity tests and comparisons with SESAME-79 data, *J. Appl. Meteorol.*, *21*, 1594–1608.

T. A. Black, Biometeorology and Soil Physics Group, Faculty of Land and Food Systems, University of British Columbia, 2357 Main Mall, Vancouver, BC, V6T 1Z4, Canada.

B. Chen, J. M. Chen, and G. Mo, Department of Geography and Program in Planning, University of Toronto, ON, M5S 3G3, Canada. (chenb@geog.utoronto.ca)